Push-and-pull regulation of the fusion pore by synaptotagmin-7

Margarita Segovia[a,1], Eva Alés[a,1], María Angeles Montes[a], Imelda Bonifas[a,2], Imane Jemal[a], Manfred Lindau[b], Anton Maximov[c,d,e,f,3], Thomas C. Südhof[c,d,e,f,4], and Guillermo Alvarez de Toledo[a,4]

[a]Departamento de Fisiología Médica y Biofísica, Facultad de Medicina, University of Seville, 41009 Seville, Spain; [b]School of Applied and Engineering Physics, Cornell University, Ithaca, NY 14853; [c]Department of Cellular and Molecular Physiology and [d]Howard Hughes Medical Institute, Stanford University School of Medicine, Palo Alto, CA 94304; and [e]Department of Neuroscience and [f]Howard Hughes Medical Institute, University of Texas Southwestern Medical Center, Dallas, TX 75390

In chromaffin cells, Ca^{2+} binding to synaptotagmin-1 and -7 triggers exocytosis by promoting fusion pore opening and fusion pore expansion. Synaptotagmins contain two C2 domains that both bind Ca^{2+} and contribute to exocytosis; however, it remains unknown whether the C2 domains act similarly or differentially to promote opening and expansion of fusion pores. Here, we use patch amperometry measurements in WT and synaptotagmin-7–mutant chromaffin cells to analyze the role of Ca^{2+} binding to the two synaptotagmin-7 C2 domains in exocytosis. We show that, surprisingly, Ca^{2+} binding to the C2A domain suffices to trigger fusion pore opening but that the resulting fusion pores are unstable and collapse, causing a dramatic increase in kiss-and-run fusion events. Thus, synaptotagmin-7 controls fusion pore dynamics during exocytosis via a push-and-pull mechanism in which Ca^{2+} binding to both C2 domains promotes fusion pore opening, but the C2B domain is selectively essential for continuous expansion of an otherwise unstable fusion pore.

patch amperometry | synaptic transmission | capacitance measurements | neurotransmitter release | patch clamp

In neurons and neuroendocrine cells, secretion is induced by Ca^{2+}-dependent fusion of synaptic vesicles or secretory granules (1–3). Fusion in each case is triggered by Ca^{2+} binding to synaptotagmins, with synaptic vesicle fusion being mediated by synaptotagmin-1, -2, or -9 (Syt1, Syt2, or Syt9), and secretory granule fusion in chromaffin cells by Syt1 and Syt7 (4–9). Synaptotagmins are secretory vesicle membrane proteins composed of an N-terminal transmembrane region and two C-terminal C2 domains, C2A and C2B, each of which binds Ca^{2+} (10–12). In chromaffin cells, KO of Syt1 alone abolishes the fast phase of exocytosis (7, 8), whereas double KO of Syt1 and Syt7 abolishes all major phases of exocytosis, which together account for more than 90% of Ca^{2+}-triggered fusion (9). Similar results were obtained for Syt1, Syt7, and Syt9 in other neuroendocrine cells (13–18).

Synaptotagmins probably promote fusion pore opening and expansion during exocytosis, but it is unclear whether they sculpt the fusion pore directly or control fusion pore dynamics indirectly. Synaptotagmins act in exocytosis by Ca^{2+}-dependent binding to SNARE proteins and phospholipids (19–22). Strikingly, the two C2 domains perform differential functions in exocytosis: Whereas Ca^{2+} binding to the Syt1 C2B domain is essential for exocytosis, Ca^{2+} binding to the C2A domain boosts C2B-domain action approximately twofold but in itself is not essential (23–25). However, it remains unknown how the two C2 domains differentially affect fusion pore dynamics to account for their overall functions in exocytosis.

Most studies on synaptotagmins were carried out in synapses, where fusion pores cannot be monitored accurately. Neuroendocrine cells allow a more reliable analysis of fusion pores, and much has been learned about synaptotagmin function in native chromaffin cells and in transfected and/or permeabilized PC12 cells (8, 9, 13–15, 22, 26–30). However, the differential role of C2 domains in fusion pores was studied only in overexpression studies in transfected PC12 cells, in which Syt1 overexpression paradoxically inhibits exocytosis (26). Although these studies confirmed that the Syt1 C2 domains perform distinct functions in fusion (27–29), overexpression can produce general changes in membrane dynamics and promote unphysiological protein inter-

actions [as evidenced by the overexpression-induced inhibition of fusion by Syt1 (26)], rendering interpretations difficult. Thus, to tease apart the physiological role of the C2 domains of a synaptotagmin in fusion-pore dynamics, analyses that substitute the endogenous protein at physiological levels are required.

In the present study, we used Syt7 KO and knockin (KI) mice that either lack Syt7 expression or express at physiological levels mutant Syt7 with point mutations that abolish Ca^{2+} binding to its C2B domain (Syt7* KI) (31). Using cultured chromaffin cells from these mice, we examined the role of the Syt7 C2 domains in fusion pore opening and expansion. Because a potential problem in analyzing fusion pores is the difficulty in measuring fusion pore dynamics using only conventional techniques such as amperometry, we also used patch amperometry (32), the only method that allows reliable biophysical measurements of fusion pore dynamics in a neuroendocrine cell. Patch amperometry simultaneously detects the increase in cell-surface area caused by the fusion of a single secretory granule and electrochemically detects catecholamine release by means of a carbon fiber detector inserted inside a patch pipette (32). Our results show that Syt7 shapes fusion pore dynamics without directly participating in the fusion pore itself and that its C2A and C2B domains contribute differentially to the fusion pore. Ca^{2+} binding to both C2 domains opens the pore, but only Ca^{2+} binding to the C2B domain can support full expansion of the fusion pore. Our results suggest a biophysical rationale for the selectively essential role of the synaptotagmin C2B domains and provide a model of synaptotagmin function in fusion-pore dynamics under physiological expression levels of this protein.

Results

Syt7 Mediates Catecholamine Exocytosis. Ca^{2+}-triggered exocytosis of chromaffin granules was elicited by consecutive 20-s puffs of a solution containing 70 mM K^+ in the vicinity of cultured chromaffin cells and was measured by carbon-fiber amperometry (Fig. 1 A–C) (33). K^+ stimulation induced bursts of amperometric spikes that declined with repetitive stimulations, as illustrated by calculating the integrated amperometric charge under each response (Fig. 1D). Both Syt7 KO and Syt7* KI cells exhibited a decrease of ~50% in the integrated amperometric charge compared with WT cells (Fig. 1D). Thus, consistent with a previous report (9), both Syt7 mutations caused a similar ~50% inhibition of Ca^{2+}-triggered release in chromaffin cells.

Strikingly, the shape and pattern of amperometric spikes differed between WT, Syt7 KO, and Syt7* KI cells. Syt7 KO cells exhibited a decrease in the number of spikes per stimulus compared with WT cells (Fig. 1E), whereas Syt7* KI cells displayed an increase in the number of spikes (WT cells: 39 ± 5 spikes/K$^+$ stimulus, $n = 24$ cells; Syt7 KO cells: 29 ± 5 spikes/K$^+$ stimulus, $n = 16$ cells; Syt7* KI cells: 68 ± 12 spikes/K$^+$ stimulus, $n = 24$ cells; $P = 0.00238$ and $P = 0.0208$, for KI/KO and KI/WT comparisons, respectively). In contrast, the average half-width of individual spikes was similar for WT and Syt7 KO cells [10.76 ± 1.06 ms ($n = 2,564$ spikes/38 cells) and 10.35 ± 0.87 ms ($n = 2,275$ spikes/48 cells), respectively] but was much lower in Syt7* KI cells (5.93 ± 0.29 ms; $n = 3,826$ spikes/55 cells) (Fig. 1F). As a result, the average charge per spike (pC) was 0.62 ± 0.086 in WT cells, 0.49 ± 0.053 in Syt7 KO cells, and 0.33 ± 0.022 Syt7* KI cells (Fig. 1G), indicating that smaller amounts of catecholamines are released per fusion event in Syt7* KI cells. Thus, although the cumulative charge of spikes was decreased to the same extent in Syt7 KO and Syt7* KI cells, as compared with WT cells (Fig. 1D), the mechanism of the decrease differs: Syt7 KO cells execute fewer exocytic events that, however, have WT properties, whereas Syt7* KI cells execute more exocytic events that, however, release smaller amounts of catecholamines per event.
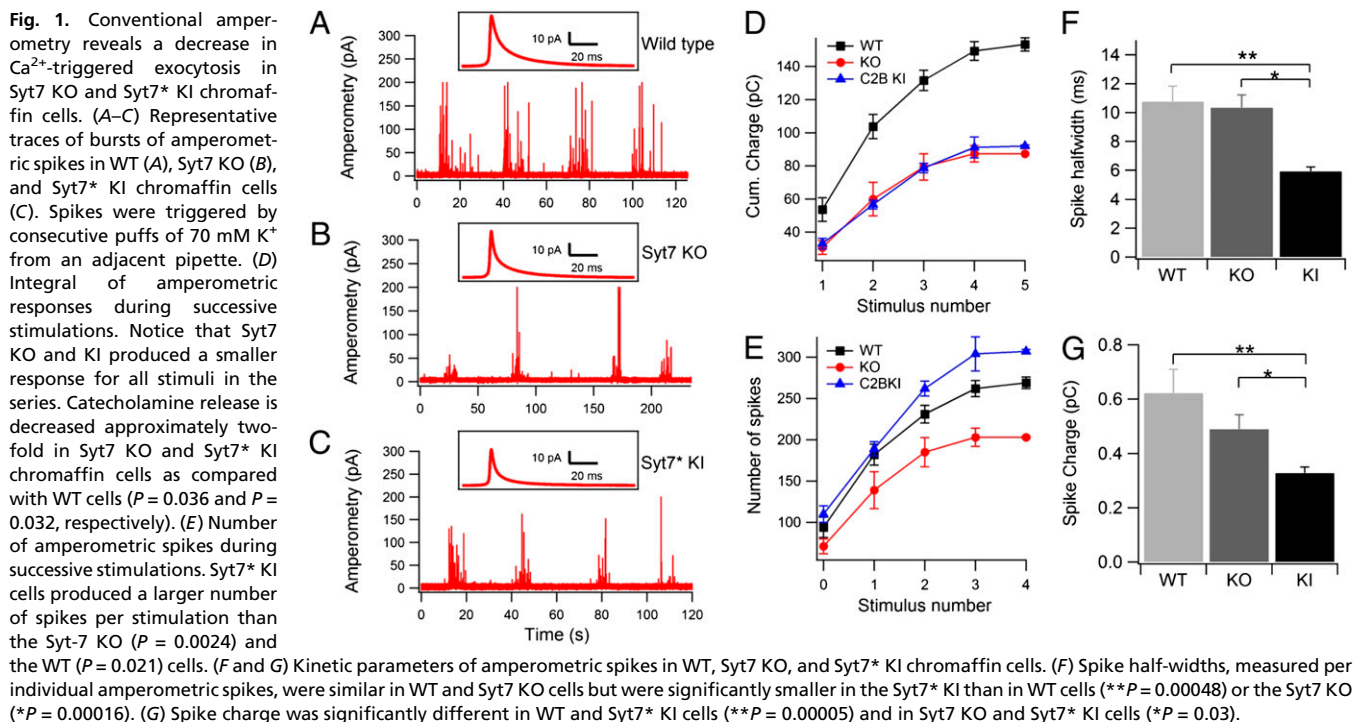
Syt7 Mutations Do Not Alter the Kinetics of Fusion-Pore Opening. We next examined foot signals preceding amperometric spikes because the parameters of these amperometric feet (e.g., their duration, amplitude, and charge) provide insight into the properties of exocytic fusion pores (33, 34). We measured the foot from the time at which the amperometric current exceeds noise by 3 SD until the development of the upstroke of the amperometric spike (by extrapolation to zero from the rising phase of the amperometric spike) (Fig. 2A). To monitor specifically the spikes originating close to the surface of the electrochemical detector, we examined only spikes with amplitudes >20 pA. The distribution of foot duration times could be fitted by a single exponential (Fig. 2 B–D), although an additional slower exponential component might be present in WT and Syt7 KO cells that was not studied further (see upward deviation of data points for long-lasting feet in Fig. 2 B and C). We observed no significant differences in foot duration in WT (7.05 ± 0.92 ms, $n = 29$ cells), Syt7 KO (6.6 ± 0.79 ms, $n = 16$ cells), and Syt7* KI cells (7.4 ± 0.78 ms, $n = 36$ cells) (Fig. 2E), nor were the foot amplitudes (Fig. 2F) and charges (Fig. 2G) significantly

different, suggesting that Syt7 does not affect the structure and dynamics of the early exocytic fusion pore.

Patch Amperometry Measurements from Syt7 KO Cells. To define better the biophysical properties of fusion pores in Syt7 KO and KI cells, we performed patch amperometry experiments (Fig. 3A). By simultaneously measuring the capacitance of a membrane patch and the exocytic release of catecholamines in this patch, patch amperometry allows high-resolution definitions of fusion pores (32, 34–37). Although patch amperometry monitors exocytic events that occur spontaneously in response to sealing the patch pipette on the cell surface, the fusion events observed nevertheless are Ca^{2+}-dependent and are triggered by the Ca^{2+} introduced into the cell during patching (34).

An example of stepwise increases in capacitance, indicating full fusion of chromaffin granules with the membrane patch under the pipette tip, is shown by the blue trace in Fig. 3B. Exocytosis of catecholamines into the patch pipette is measured as an amperometric spike that follows the step increase in capacitance (Fig. 3B, red trace). The amplitude of the amperometric spike peak varies among exocytic events but correlates with the size of the capacitance step, indicating that larger chromaffin granules contain a higher amount of catecholamines, although all chromaffin granules contain a similar concentration of catecholamines (37). Events detected by patch amperometry are slower than the events observed by conventional amperometry, presumably because the distance from the carbon fiber electrode (CFE) to the membrane is slightly longer in the patch amperometry than in the conventional amperometry configuration.

We observed no significant difference in the size of capacitance steps in WT, Syt7 KO, and Syt7* KI cells (Fig. 3C), demonstrating that the size of chromaffin granules was unchanged in Syt7 KO and KI cells. Thus, the reduced charge of individual amperometric spikes (Fig. 1G) in Syt7* KI cells is not caused by a change in vesicle size. This reduction could be caused by a lower catecholamine concentration inside the vesicles or by partial release in individual fusion events. If the smaller amperometric spike charges are associated with unchanged stepwise increases in cell surface area (full fusion) (Fig. 3B), the vesicular catecholamine concentration probably is decreased. If, conversely, smaller amperometric spike charges are associated with transient increases in the cell surface area ("flickers"), the fusion events probably are

Fig. 1. Conventional amperometry reveals a decrease in Ca^{2+}-triggered exocytosis in Syt7 KO and Syt7* KI chromaffin cells. (A–C) Representative traces of bursts of amperometric spikes in WT (A), Syt7 KO (B), and Syt7* KI chromaffin cells (C). Spikes were triggered by consecutive puffs of 70 mM K$^+$ from an adjacent pipette. (D) Integral of amperometric responses during successive stimulations. Notice that Syt7 KO and KI produced a smaller response for all stimuli in the series. Catecholamine release is decreased approximately two-fold in Syt7 KO and Syt7* KI chromaffin cells as compared with WT cells ($P = 0.036$ and $P = 0.032$, respectively). (E) Number of amperometric spikes during successive stimulations. Syt7* KI cells produced a larger number of spikes per stimulation than the Syt-7 KO ($P = 0.0024$) and the WT ($P = 0.021$) cells. (F and G) Kinetic parameters of amperometric spikes in WT, Syt7 KO, and Syt7* KI chromaffin cells. (F) Spike half-widths, measured per individual amperometric spikes, were similar in WT and Syt7 KO cells but were significantly smaller in the Syt7* KI than in WT cells (**$P = 0.00048$) or the Syt7 KO (*$P = 0.00016$) cells. (G) Spike charge was significantly different in WT and Syt7* KI cells (**$P = 0.00005$) and in Syt7 KO and Syt7* KI cells (*$P = 0.03$).
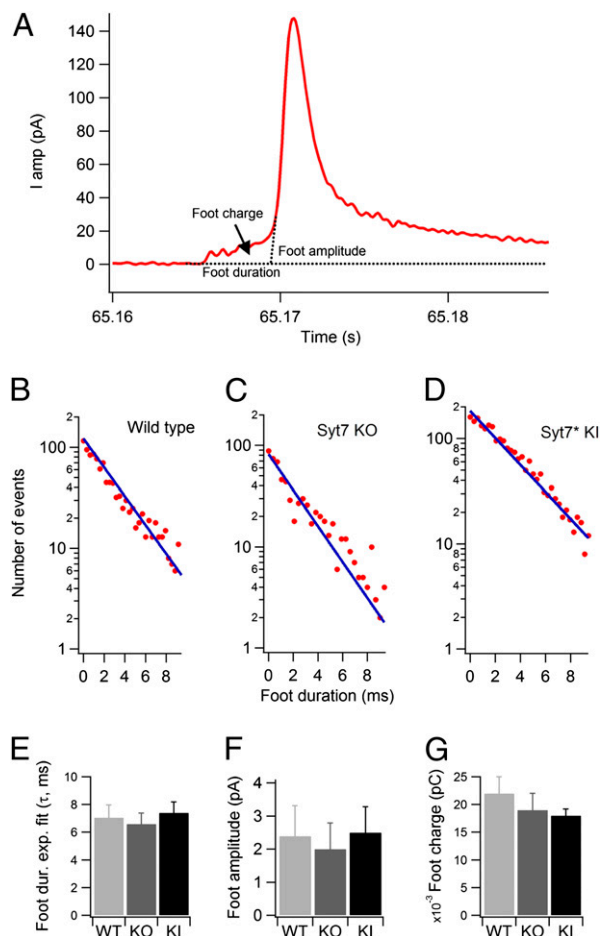
NEUROSCIENCE

Fig. 2. Analysis of amperometric feet events suggest normal fusion-pore opening in Syt7 KO and Syt7* KI chromaffin cells. (*A*) Representative trace of an amperometric spike induced by a puff of 70 mM K+ to illustrate analysis of amperometric feet. Foot onset was detected when the amperometric signal exceeded noise by 3 SD. Foot duration was calculated from the point of foot onset to the point of spike initiation obtained by extrapolating the upstroke of the spike to the baseline. (*B–D*) Foot durations, determined by the onset of amperometric signals that exceeded noise by 3 SD, and the initiation of the amperometric spike, determined by extrapolating the upstroke of the spike to the baseline, in WT (*B*), Syt7 KO (*C*), and Syt7* KI (*D*) chromaffin cells. Durations of Individual feet were plotted on a semilogarithmic scale and fitted to a straight line to determine the time constant of the dwell-time distribution of feet events shown in the graph. (*E–G*) Average fitted time-constant values in different cells of foot duration (*E*), foot amplitudes (*F*), and foot charge (*G*). In this parameter, no significant differences were observed in WT (*n* = 29), Syt7 KO (*n* = 16), and Syt7 KI (*n* = 36) cells.

transient and do not allow full release of the granule contents. Indeed, we observed that the charge of amperometric spikes associated with capacitance steps (i.e., full-fusion events) was similar for WT and Syt7 KO cells [3.24 ± 0.5 pC (*n* = 209 spikes/20 cells) and 3.8 ± 0.4 pC (*n* = 183 spikes/16 cells), respectively], indicating that the vesicular catecholamine concentration was unchanged in Syt7 KO cells (Fig. 3D). The charge associated with capacitance steps also was not statistically significant in Syt7* KI cells compared with WT cells (2.7 ± 0.3 pC; *n* = 272 spikes/20 cells). Thus, the vesicular catecholamine concentrations are not significantly different. Other kinetic parameters determined in patch amperometry are shown in Table S1.

Ca²⁺ Binding to the Syt7 C2B Domain Promotes Fusion-Pore Expansion. We next analyzed the fusion pore conductance of full-fusion events in WT, Syt7 KO, and Syt7* KI cells to test whether the Syt7 mutations alter fusion pore properties, especially fusion pore expansion (Fig. 4). From the imaginary (Im; blue traces in Fig. 4A and
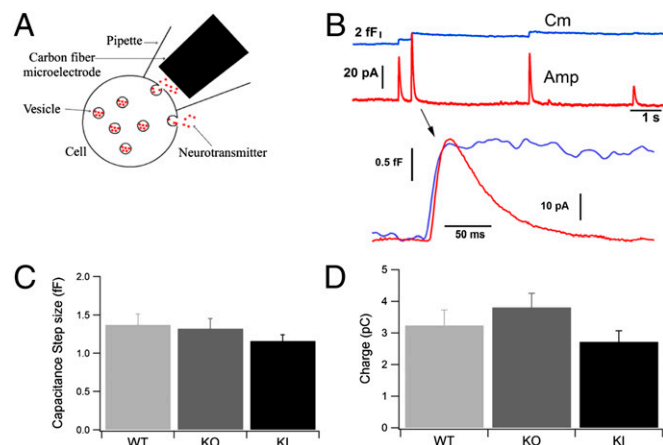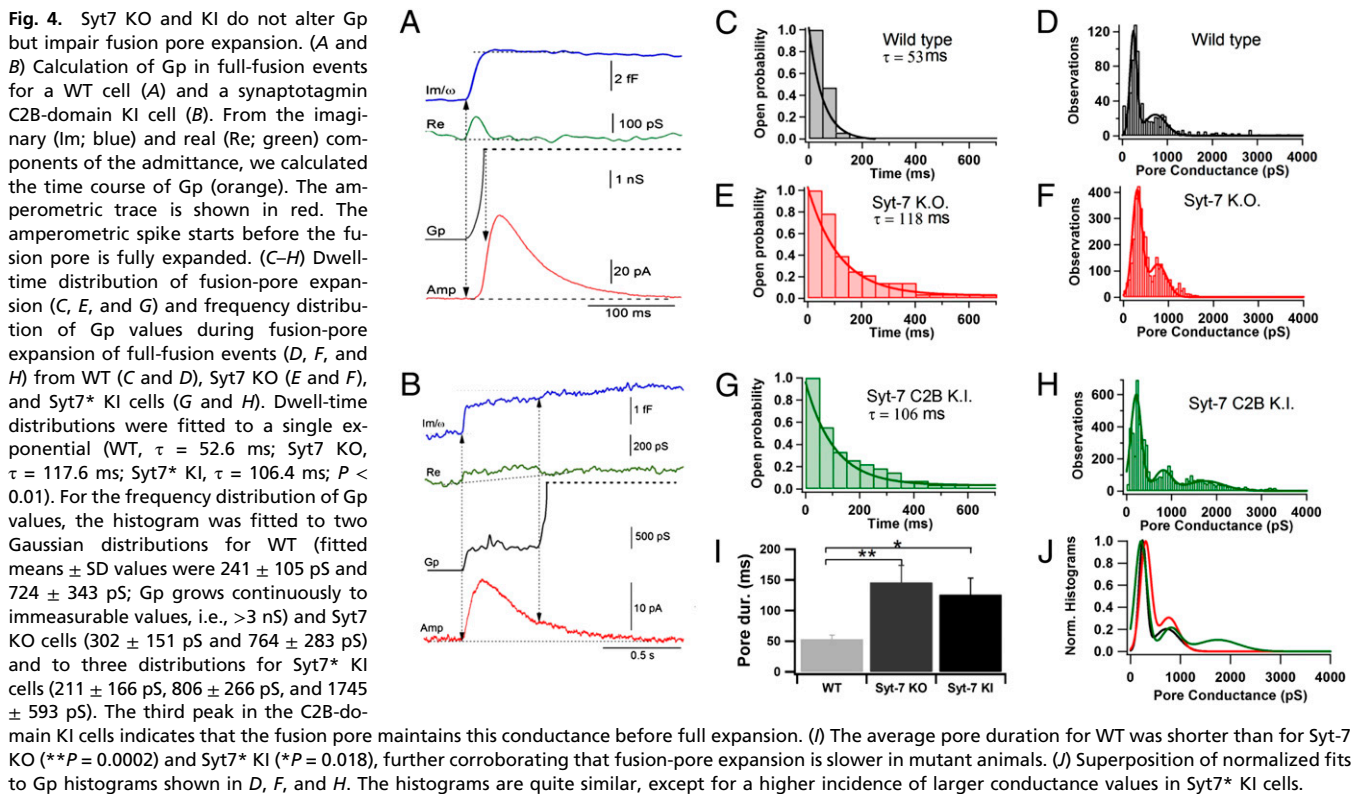

Fig. 3. Patch amperometry of single full-fusion exocytotic events in Syt7 mutants. (*A*) Patch amperometry configuration. On-cell patch clamping is achieved with a pipette containing a CFE. The cell membrane capacitance can be measured with a resolution that detects fusion of a single chromaffin granule with the membrane patch. Release of catecholamines into the patch pipette by spontaneous exocytotic events is measured electrochemically with the CFE. Catecholamine release occurring over the rest of the cell surface is not detected. (*B*) (*Upper*) Representative traces (example depicts a WT cell) showing simultaneous measurements of step increase in capacitance (blue trace) and of amperometric spike (red trace). (*Lower*) In the expanded exocytotic event, notice the delay between the onset of the capacitance and amperometric increase. (*C*) The size of the capacitance steps induced by exocytosis of individual chromaffin granules was similar for WT, Syt7 KO, and Syt7* KI cells (*P* > 0.05). (*D*) The charge in individual amperometric spikes associated with full-fusion events as detected by capacitance was similar for WT (3.2 ± 0.5 pC) and Syt7 KO cells (3.8 ± 0.4 pC, *P* > 0.05) but decreased slightly in Syt7* KI cells (2.7 ± 0.3 pC) compared with Syt7 KO cells, consistent with the reduced charge measured in Syt7* KI cells by conventional extracellular amperometry.

B) and real (Re; green traces) components of the admittance, we determined the fusion pore conductance. Pore conductance (Gp, black traces), which we correlated with catecholamine release as measured by amperometry (red), was calculated using the equation Gp = (Re² + Im²)/Re (35). In a typical example from a WT cell, fusion pores expanded rapidly (Fig. 4A), and most full-fusion events reached an immeasurable Gp value quickly. In Syt7* KI cells, as shown in a characteristic example in Fig. 4B, the time course of Gp occasionally showed a long plateau, in this case with a fusion-pore conductance of ~450 pS, before completely opening (black trace). Interestingly, during this plateau phase a clear but slow amperometric spike was detected (red trace), indicating rather complete release of the vesicle contents via a narrow fusion pore.

We defined fusion-pore expansion as full when Gp was >2 nS and plotted the frequency distribution of fusion pore lifetimes from opening until full fusion pore expansion was reached. In WT cells, this distribution followed an approximately exponential distribution, with a time constant of 53 ms (Fig. 4C), suggesting that a single rate-limiting step controls fusion pore expansion. In both Syt7 KO and Syt7* KI cells, however, we observed a significant number of narrow, low-conductance fusion pores that exhibited longer lifetimes than in WT cells (Fig. 4B). As a result, the fitted time constants for the lifetime distribution of fusion pore opening were twofold larger in Syt7 KO (118 ms) and Syt7* KI cells (106 ms) than in WT cells (53 ms) (Fig. 4 *C*, *E*, and *G*). To calculate this difference more accurately, we determined the average lifetime of fusion pores in individual cells and then calculated the mean of the average lifetimes (Fig. 4I) (WT: 53 ± 7 ms, *n* = 17 cells; Syt7 KO: 146 ± 28 ms, *n* = 28 cells; Syt7* KI: 126 ± 27 ms, *n* = 27 cells; WT/Syt7 KO, *P* = 0.0002; WT/Syt7* KI, *P* = 0.018). The average lifetime is even longer for Syt7 KO and Syt7* KI cells because of the contribution of some long-lasting events. Thus, both Syt7 KO and Syt7* KI mutations delay fusion pore expansion. We must point out the apparent inconsistency of this finding with the unchanged foot duration observed in the amperometry experiments.

Fig. 4. Syt7 KO and KI do not alter Gp but impair fusion pore expansion. (*A* and *B*) Calculation of Gp in full-fusion events for a WT cell (*A*) and a synaptotagmin C2B-domain KI cell (*B*). From the imaginary (Im; blue) and real (Re; green) components of the admittance, we calculated the time course of Gp (orange). The amperometric trace is shown in red. The amperometric spike starts before the fusion pore is fully expanded. (*C–H*) Dwell-time distribution of fusion-pore expansion (*C*, *E*, and *G*) and frequency distribution of Gp values during fusion-pore expansion of full-fusion events (*D*, *F*, and *H*) from WT (*C* and *D*), Syt7 KO (*E* and *F*), and Syt7* KI cells (*G* and *H*). Dwell-time distributions were fitted to a single exponential (WT, τ = 52.6 ms; Syt7 KO, τ = 117.6 ms; Syt7* KI, τ = 106.4 ms; *P* < 0.01). For the frequency distribution of Gp values, the histogram was fitted to two Gaussian distributions for WT (fitted means ± SD values were 241 ± 105 pS and 724 ± 343 pS; Gp grows continuously to immeasurable values, i.e., >3 nS) and Syt7 KO cells (302 ± 151 pS and 764 ± 283 pS) and to three distributions for Syt7* KI cells (211 ± 166 pS, 806 ± 266 pS, and 1745 ± 593 pS). The third peak in the C2B-domain KI cells indicates that the fusion pore maintains this conductance before full expansion. (*I*) The average pore duration for WT was shorter than for Syt-7 KO (**P = 0.0002) and Syt7* KI (*P = 0.018), further corroborating that fusion-pore expansion is slower in mutant animals. (*J*) Superposition of normalized fits to Gp histograms shown in *D*, *F*, and *H*. The histograms are quite similar, except for a higher incidence of larger conductance values in Syt7* KI cells.

A fusion-pore conductance measurement has a time resolution of 4–12 ms (for the 1–3 ms, 24 dB lock-in filter setting), which is the upper limit of foot duration. Therefore, admittance measurements selectively monitor a subset of fusion-pore lifetimes indicated by the amperometric foot signals analyzed in conventional amperometric recordings as in Fig. 2. Syt7 appears to be selectively involved in the expansion of fusion pores with long duration.

To define better the effects of the Syt7 mutations on fusion-pore properties, we next plotted the frequency distribution of Gp values measured during fusion pore expansion in WT, Syt7 KO, and Syt7* KI cells (Fig. 4 *D*, *F*, and *H*). Similar peaks in Gp values were observed in WT, Syt7 KO, and Syt7* KI cells (250 pS, 300 pS, and 200 pS, respectively). The frequency distributions of Gp values show larger additional peaks around 760–800 pS, indicating that fusion-pore expansion is not a continuous process. Together, these results indicate that the structure of the early fusion pore is unchanged in Syt7 KO and KI cells, consistent with the lack of change in the amperometric foot signals (Fig. 2), but that fusion pores dwell longer in a partly opened state in Syt7 mutant cells.

Syt7* KI Increases Kiss-and-Run Events. In patch amperometry of WT cells, we observe not only full-fusion events characterized by stepwise capacitance changes but also occasional capacitance flickers in which the capacitance increase is rapidly reversed but still is associated with an amperometric signal. Strikingly, we detected a large increase in the incidence of such capacitance flickers in Syt7* KI cells (Fig. 5 *A* and *B*). Moreover, we occasionally observed amperometric spikes without any apparent change in capacitance trace, presumably reflecting transient fusion events of a duration that is too short for the time resolution of the capacitance measurements (4–12 ms, depending on lock-in filter setting). In most cases, we could record a change in the real part of the admittance during capacitance flickers, reflecting the initial narrow fusion pore. A simulation further supporting the notion that these events are caused by a transient fusion pore of 100–150 pS is shown in Fig. S1, suggesting that the capacitance flickers represent rapid kiss-and-run fusion events with release via a brief transient opening of the fusion pore.

Fig. 5*C* plots the relationship between the amplitude of capacitance increases and the amplitude of the amperometric spike.

The red dots represent full-fusion events, indicating a linear relationship between these two parameters, as has been described (23–25). Green triangles show the same relationship for transient fusion events. Note that the charge of the spikes for which the change in capacitance was undetectable (volume of zero) was smaller, on average, than that of spikes where a capacitance change was observed. In most cases, we could record a change in the real part of the admittance, reflecting an initial narrow fusion pore. This observation is in agreement with a reduced quantal size of events in Syt7* KI cells in regular amperometry experiments, because part of the vesicle contents might be lost during spontaneous or potassium-induced kiss-and-run events. The amount of catecholamine released during kiss-and-run events was significantly smaller than in full-fusion events (Fig. 5*D*). This effect was even more pronounced in kiss-and-run events that showed very little change in capacitance (Fig. 5*D*), further indicating partial release of the vesicle contents through a small fusion pore.

Finally, we analyzed the relative proportion of transient fusion and full-fusion events in WT, Syt7 KO, and Syt7* KI cells. The percentages of full-fusion and kiss-and-run events per cell were similar for WT and Syt7 KO cells [full fusion: WT, 77.8 ± 5% (*n* = 12 cells, 414 events); Syt7 KO, 79.8 ± 3.4% (*n* = 12 cells, 358 events); kiss-and-run events: WT, 22.2 ± 5% (*n* = 12 cells, 118 events); Syt7 KO, 20.2 ± 3.4% (*n* = 12 cells, 78 events)]. In contrast, the percentage of full-fusion events exhibited a significant decrease in Syt7* KI cells (59.1 ± 5.3%; *n* = 23 cells, 441 events), whereas the percentage of kiss-and-run events doubled [40.9 ± 5.3% (*n* = 23 cells, 265 events); WT/Syt7* KI, *P* = 0.02; Syt7 KO/Syt7* KI, *P* = 0.0074]. Accordingly, the ratio of kiss-and-run to full-fusion events for individual cells was increased significantly in Syt7* KI cells (0.91 ± 0.14; *n* = 23 cells) as compared with WT cells (0.38 ± 0.14; *n* = 12 cells; *P* = 0.02) or Syt7 KO cells (0.28 ± 0.06; *n* = 12 cells; *P* = 0.0074) (Fig. 5*E*). During kiss-and-run events, the distribution of Gp was shifted to smaller conductance values (Fig. 5*F*). The lifetime of the fusion pore while flickering was 73 ms and was comparable to the time taken by the fusion pore to expand in full-fusion events (Fig. 5*G*). The analysis of transient fusion events was done only in the Syt7* KI cells, because these events are so rare in WT and Syt7 KO cells that we could not collect sufficient data for analysis.
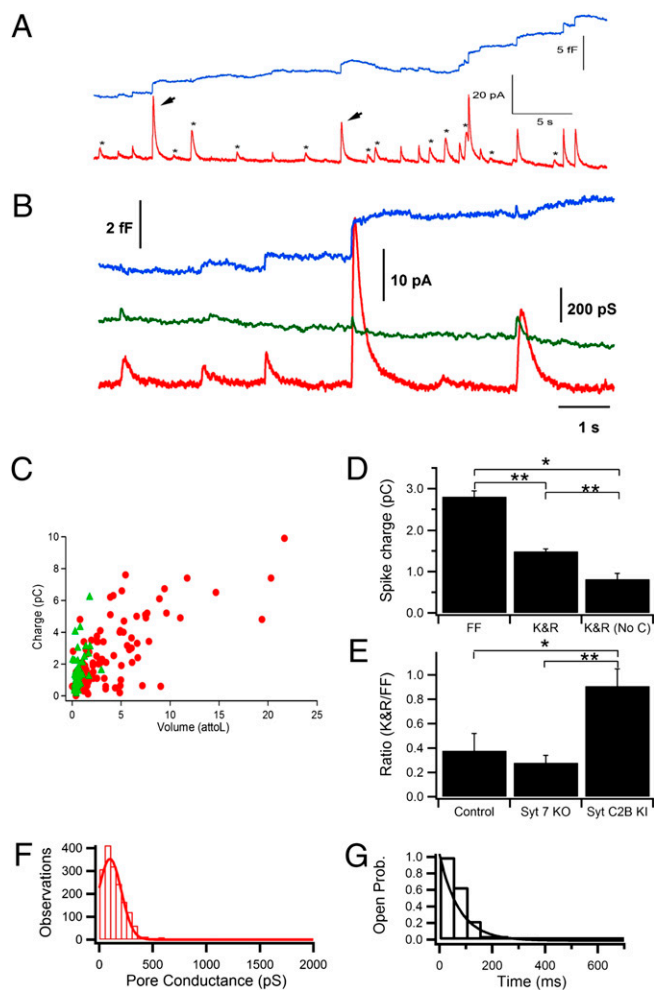
Fig. 5. Patch amperometry of fusion-pore expansion: full collapse of fused vesicles vs. kiss-and-run fusion. (*A* and *B*) Spontaneous release events as detected by cell-membrane capacitance and amperometry in Syt7* KI chromaffin cells. Traces show step changes in capacitance (blue) and conductance (green) resulting from the fusion of a single chromaffin granule with the plasma membrane. Amperometric spikes (red) coincide with the step changes in capacitance (arrows in *A*). Smaller amperometric spikes can be seen between capacitance steps (asterisks in *A*). The first seconds of the recording shown in *A* are illustrated in an expanded time scale in *B*. In some of these spikes, we observed a transient increase in the capacitance and conductance traces, consistent with a flickering fusion event. (*C*) Relationship between amperometric spike charge and vesicle volume as calculated from the change in capacitance. Dots represent step changes in capacitance; triangles represent the capacitance increase during transient fusion events. Some spikes did not show any change in capacitance (triangles over zero volume). (*D*) Amperometric charge during full-fusion (FF) and kiss-and-run (K&R) events as determined in Syt7* KI cells. Kiss-and-run events with an observable change in capacitance had a significantly smaller charge than full-fusion events. Smaller amounts of catecholamines were released in kiss-and-run events with no observable change in capacitance (K&R no C) than in full-fusion events. Kiss-and-run events with no change in capacitance had a significantly smaller amperometric charge than kiss-and-run events in which we could detect a change in capacitance, further indicating partial release during kiss-and-run events. *$P < 0.0001$; **$P = 0.002$. (*E*) Ratio of kiss-and-run and full-fusion events for WT, Syt7 KO, and Syt7* KI cells. The proportion of full-fusion events decreases in Syt7* KI versus the WT and Syt7 KO cells; Kiss-and-run events increase concomitantly in Syt7* KI with respect to WT and Syt7 KO cells. *$P = 0.02$; **$P = 0.0074$. (*F* and *G*) Fusion-pore analysis for reversible fusion events in Syt7* KI cells. (*F*) Gp distribution is skewed to the left in reversible fusion events as compared with full-fusion events, indicating fusion pores that do not dilate during kiss-and-run events. (*G*) The dwell-time distribution of fusion-pore opening has a τ of 73 ms.

Discussion

Using conventional amperometry to study the K^+-stimulated fusion of single granules in cultured chromaffin cells, we show that both Syt7 KO and Syt7* KI cells reduce release by ~50% but do so by different mechanisms (Fig. 1). Syt7 KO cells decrease the rate of fusion events, with no change in quantal size. In contrast, Syt7* KI cells decrease the quantal size of fusion events, with no change in their rate. Moreover, analyses of amperometric feet showed that neither Syt7 mutation altered the kinetics of fusion pore opening (Fig. 2). These observations confirm that Syt7, together with Syt1, mediates the Ca^{2+} triggering of fusion pore opening in chromaffin cells (9) and suggest, somewhat surprisingly, that Ca^{2+} binding to the C2A domain is fully sufficient to trigger fusion pore opening when the C2B domain is blocked from Ca^{2+} binding. Indeed, the loss of overall Syt7 function in the Syt7* KI cells that lack Ca^{2+} binding to the C2B domain appears to be caused by a decrease in the amounts of catecholamines released by individual fusion events, as reflected in the large decrease in quantal size that is observed as a decrease in amperometric spike halfwidth in Syt7* KI cells but not in Syt7 KO cells (Fig. 1).

To determine why Syt7* KI cells exhibit not a simple decrease in fusion events but a shift to less productive fusion events and why Ca^{2+} binding to the C2B domain is essential for normal fusion-pore formation, we performed patch amperometry experiments (Fig. 3). We found that the Syt7 KO and Syt7* KI mutations did not change the conductance properties of the fusion pore (Fig. 4). This result is important, because it suggests that Syt7 and, by extension, other synaptotagmins as well, do not contribute directly to the fusion-pore structure but instead modulate it via Ca^{2+}-triggered phospholipid and SNARE binding. We did observe, however, that both the Syt7 KO and the Syt7* KI mutation dramatically retarded the expansion of long-lived fusion pores, as evidenced by a twofold-longer average fusion pore expansion time (Fig. 4). This function of Syt7 is observed selectively for long-lived fusion pores and is not evident in rapidly expanding fusion pores that dominate the foot duration in conventional amperometric recordings. Finally, we found that the Syt7* KI cells, but not the Syt7 KO cells, dramatically increased the relative frequency of unstable fusion pores, resulting in an increase in the frequency of transient events.

A plausible model to account for our observations, on the background of the literature, is that synaptotagmins in general and Syt7 in particular function in a two-stage manner. Ca^{2+} binding to both C2 domains promotes initial fusion pore opening, with Ca^{2+} binding to the C2A domain alone being sufficient for this action, as indicated by the fact that inactivation of Ca^{2+} binding to the C2B domain in Syt7* KI cells does not decrease the number of Ca^2 $^+$-triggered fusion events observed by amperometry (Fig. 1). Thus, although Ca^{2+} binding to the C2B domain is essential for normal exocytosis (23–25), it actually is not required for initiating fusion, and Ca^{2+} binding to the C2A domain alone suffices to pull open the fusion pore via a Ca^{2+}-dependent restructuring of the phospholipid membranes with associated SNARE–protein complexes. However, Ca^{2+} binding to the C2B domain is essential for stabilizing fusion pores once they have opened, as evidenced by the enormous increase in transient fusion pores in Syt7* KI cells (Fig. 5).

Can this model account for all the present observations on the function of synaptotagmin C2 domains, not only those described in the present study but also those of previous studies? A major implication of the model is that the well-documented essential nature of Ca^{2+} binding to the C2B domain (23–25) does not reflect its role in initiating initial fusion pore opening (which it must do, similar to Ca^{2+} binding to the C2A domain, because C2A-domain mutants block only ~50% of synaptotagmin function) (25) but is the result of the role of Ca^{2+} binding to the C2B domain in promoting productive fusion pore openings. Thus, the overall decrease in fusion events in Syt7 KO cells would be caused by decreased fusion pore opening events, with the remaining 50% of fusion events caused by Syt1 (9). Moreover, our study contains two key observations that are puzzling but can be explained by our model. First, fusion events in Syt7* KI cells release smaller amounts of catecholamines than fusion events in either WT or Syt7 KO cells, even though the size of the capacitance steps is unchanged (and thus the granules are not smaller) (Figs. 1 and 3). Given the high incidence of transient fusion pores without full collapse in Syt7* KI cells, the most likely explanation for this observation is that the reduced quantal size could be

caused by a partial release in the form of kiss-and-run events. Second, both the Syt7 KO and the Syt7* KI mutation increase the dwell time of the fusion pore (Fig. 4), a result that seems counterintuitive if the Syt7 KO simply produced fewer but otherwise normal fusion events mediated by Ca^{2+} binding to Syt1. However, Ca^{2+} triggering of exocytosis probably requires activation of an unknown minimum number of synaptotagmins on a vesicle or granule. When Syt7 is inactivated in the Syt7 KO, the concentration of activated synaptotagmins on chromaffin granules is lower, because only Syt1 is left, causing the decrease not only in fusion-pore opening but also in the fusion pore expansion rate.

Experimental Procedures

Chromaffin Cell Preparation. We used chromaffin cells from adult (3- to 6-mo-old) male and female Syt7 KO and Syt7* KI mice. Primary chromaffin cell cultures were prepared as previously described (37) and incubated at 37 °C at 5% CO_2. Experiments were done on cells after 1–4 d in culture at room temperature.

Solutions. The pipette solution contained 80 mM tetraethylammonium chloride, 35 mM NaCl, 5–10 mM $CaCl_2$, 1 mM $MgCl_2$, 10 mM Hepes/NaOH, 5 mM ClK, and 5 mM $BaCl_2$. The bath solution contained 140 mM NaCl, 2.7 mM KCl, 5 mM $CaCl_2$, 1 mM $MgCl_2$, 10 mM Hepes/NaOH, and 5–10 mM glucose. For regular carbon fiber amperometry, we used the following solution for stimulation: 72 mM NaCl, 70 mM KCl, 10 mM Hepes, 6 mM glucose, 4 mM $CaCl_2$, and 4 mM $MgCl_2$. For all solutions the osmolarity was 300 mOsm/kg, and the pH was adjusted to 7.4.

Generation of Syt7 Knockout and Knockin Models. The generation and analysis of Syt7-mutant mice has been described (31).

Amperometry and Patch Amperometry. Regular extracellular amperometry was performed by placing a carbon fiber electrode held at +800 mV in the vicinity of the cell as described (33). Amperometric currents were filtered with an eight-pole low-pass Bessel filter set at 3 kHz. Changes in membrane capacitance caused by single chromaffin granule fusion and catecholamine release from the same granule were recorded simultaneously by patch amperometry (32, 37). Briefly, on-

cell patch clamp gigaseals were obtained with a patch pipette containing a CFE, in which the disk surface detection of the CFE was positioned very close to the tip opening (~1–5 μm). The CFE was prepared from 5-μm-diameter carbon fibers as described previously (33). Patch pipettes were pulled in three stages with a programmable puller (P-97; Sutter Instruments) and coated with a silicone compound (Sylgard 184; Dow Corning). Pipettes were fire-polished and had a typical resistance in the bath of ~2 MΩ. Pipette resistance typically increased up to 3–4 MΩ when the CFE approached the tip opening. To place the CFE, a special holder with two Ag/AgCl electrodes was used. Amperometric currents in patch amperometry experiments also were filtered with an eight-pole low-pass Bessel filter set at 3 KHz. We subtracted the constant direct current level in the CFE to calculate the time integral of the amperometric signal. We used a patch clamp amplifier (EPC-7; HEKA-Elektronik) for cell-attached capacitance measurements. Command voltage was applied to the bath. Changes of patch admittance were measured as described previously (35, 36) with a lock-in amplifier (SR830; Stanford Research Systems) using a sine-wave amplitude of 50 mV (rms) at a frequency of 20 KHz. The output filter was set to a 1- or 3-ms time constant, 24 db. Data acquisition was done with a 16-bit A/D converter (6052-E; National Instruments) with locally written software in Igor Pro (Wavemetrics, Inc.). Fusion-pore openings were analyzed as described previously (35). Gp was calculated from the real (Re) and imaginary (Im) parts of the admittance after baseline subtraction: Gp = $(Re^2 + Im^2)/Re$.

Data Analysis. Individual spike and capacitance step processing was performed using macros for IGOR (Wavemetrics), allowing peak/step detection and integration and kinetic parameter calculations. The Kruskal–Wallis test for unpaired samples was used to establish statistical significance among the different experimental data (samples were considered significantly different when $P < 0.05$). All data were expressed as mean $\pm$ SEM from experiments representing averages of the individual cells. Presented data represent experiments performed with cells from at least three different cultures.

1. Del Castillo J, Stark L (1952) The effect of calcium ions on the motor end-plate potentials. *J Physiol* 116:507–515.
2. Katz B (1969) *The Release of Neural Transmitter Substances*, ed Katz B (Liverpool Univ Press, Liverpool), p 60.
3. Sudhof TC (2004) The synaptic vesicle cycle. *Annu Rev Neurosci* 27:509–547.
4. Geppert M, et al. (1994) Synaptotagmin I: A major Ca2+ sensor for transmitter release at a central synapse. *Cell* 79:717–727.
5. Pang ZP, Sun J, Rizo J, Maximov A, Südhof TC (2006) Genetic analysis of synaptotagmin 2 in spontaneous and Ca2+-triggered neurotransmitter release. *EMBO J* 25:2039–2050.
6. Xu J, Mashimo T, Südhof TC (2007) Synaptotagmin-1, -2, and -9: Ca^{2+} sensors for fast release that specify distinct presynaptic properties in subsets of neurons. *Neuron* 54:567–581.
7. Voets T, et al. (2001) Intracellular calcium dependence of large dense-core vesicle exocytosis in the absence of synaptotagmin I. *Proc Natl Acad Sci USA* 98:11680–11685.
8. Sørensen JB, Fernández-Chacón R, Südhof TC, Neher E (2003) Examining synaptotagmin 1 function in dense core vesicle exocytosis under direct control of Ca^{2+}. *J Gen Physiol* 122:265–276.
9. Schonn JS, Maximov A, Lao Y, Südhof TC, Sørensen JB (2008) Synaptotagmin-1 and -7 are functionally overlapping Ca2+ sensors for exocytosis in adrenal chromaffin cells. *Proc Natl Acad Sci USA* 105:3998–4003.
10. Perin MS, Fried VA, Mignery GA, Jahn R, Südhof TC (1990) Phospholipid binding by a synaptic vesicle protein homologous to the regulatory region of protein kinase C. *Nature* 345:260–263.
11. Sutton RB, Davletov BA, Berghuis AM, Südhof TC, Sprang SR (1995) Structure of the first C2 domain of synaptotagmin I: A novel Ca^{2+}/phospholipid-binding fold. *Cell* 80:929–938.
12. Fernandez I, et al. (2001) Three-dimensional structure of the synaptotagmin 1 C2B-domain: Synaptotagmin 1 as a phospholipid binding machine. *Neuron* 32:1057–1069.
13. Fukuda M, Kowalchyk JA, Zhang X, Martin TF, Mikoshiba K (2002) Synaptotagmin IX regulates Ca2+-dependent secretion in PC12 cells. *J Biol Chem* 277:4601–4604.
14. Li Y, et al. (2007) Regulation of insulin secretion and GLUT4 trafficking by the calcium sensor synaptotagmin VII. *Biochem Biophys Res Commun* 362:658–664.
15. Lynch KL, Martin TF (2007) Synaptotagmins I and IX function redundantly in regulated exocytosis but not endocytosis in PC12 cells. *J Cell Sci* 120:617–627.
16. Gustavsson N, et al. (2008) Impaired insulin secretion and glucose intolerance in synaptotagmin-7 null mutant mice. *Proc Natl Acad Sci USA* 105:3992–3997.
17. Gauthier BR, et al. (2008) Synaptotagmin VII splice variants alpha, beta, and delta are expressed in pancreatic beta-cells and regulate insulin exocytosis. *FASEB J* 22:194–206.
18. Gustavsson N, et al. (2009) Synaptotagmin-7 is a principal Ca^{2+} sensor for Ca^{2+}-induced glucagon exocytosis in pancreas. *J Physiol* 587:1169–1178.
19. Fernández-Chacón R, et al. (2001) Synaptotagmin I functions as a calcium regulator of release probability. *Nature* 410:41–49.
20. Pang ZP, et al. (2006) Synaptotagmin-2 is essential for survival and contributes to Ca^{2+} triggering of neurotransmitter release in central and neuromuscular synapses. *J Neurosci* 26:13493–13504.
21. Rickman C, et al. (2006) Conserved prefusion protein assembly in regulated exocytosis. *Mol Biol Cell* 17:283–294.
22. Lynch KL, et al. (2008) Synaptotagmin-1 utilizes membrane bending and SNARE binding to drive fusion pore expansion. *Mol Biol Cell* 19:5093–5103.
23. Mackler JM, Drummond JA, Loewen CA, Robinson IM, Reist NE (2002) The C(2)B Ca^{2+}-binding motif of synaptotagmin is required for synaptic transmission in vivo. *Nature* 418:340–344.
24. Nishiki T, Augustine GJ (2004) Dual roles of the C2B domain of synaptotagmin I in synchronizing Ca2+-dependent neurotransmitter release. *J Neurosci* 24:8542–8550.
25. Shin OH, Xu J, Rizo J, Südhof TC (2009) Differential but convergent functions of Ca^{2+} binding to synaptotagmin-1 C2 domains mediate neurotransmitter release. *Proc Natl Acad Sci USA* 106:16469–16474.
26. Wang CT, et al. (2001) Synaptotagmin modulation of fusion pore kinetics in regulated exocytosis of dense-core vesicles. *Science* 294:1111–1115.
27. Wang CT, Bai J, Chang PY, Chapman ER, Jackson MB (2006) Synaptotagmin-Ca^{2+} triggers two sequential steps in regulated exocytosis in rat PC12 cells: Fusion pore opening and fusion pore dilation. *J Physiol* 570:295–307.
28. Bai J, Wang CT, Richards DA, Jackson MB, Chapman ER (2004) Fusion pore dynamics are regulated by synaptotagmin*t-SNARE interactions. *Neuron* 41:929–942.
29. Wang P, Chicka MC, Bhalla A, Richards DA, Chapman ER (2005) Synaptotagmin VII is targeted to secretory organelles in PC12 cells, where it functions as a high-affinity calcium sensor. *Mol Cell Biol* 25:8693–8702.
30. Shin OH, Rizo J, Südhof TC (2002) Synaptotagmin function in dense core vesicle exocytosis studied in cracked PC12 cells. *Nat Neurosci* 5:649–656.
31. Maximov A, et al. (2008) Genetic analysis of synaptotagmin-7 function in synaptic vesicle exocytosis. *Proc Natl Acad Sci USA* 105:3986–3991.
32. Dernick G, Gong LW, Tabares L, Alvarez de Toledo G, Lindau M (2005) Patch amperometry: High-resolution measurements of single-vesicle fusion and release. *Nat Methods* 2:699–708.
33. Chow RH, von Rüden L, Neher E (1992) Delay in vesicle fusion revealed by electrochemical monitoring of single secretory events in adrenal chromaffin cells. *Nature* 356:60–63.
34. Dernick G, Alvarez de Toledo G, Lindau M (2003) Exocytosis of single chromaffin granules in cell-free inside-out membrane patches. *Nat Cell Biol* 5:358–362.
35. Alvarez de Toledo G, Fernández-Chacón R, Fernández JM (1993) Release of secretory products during transient vesicle fusion. *Nature* 363:554–558.
36. Lollike K, Borregaard N, Lindau M (1995) The exocytotic fusion pore of small granules has a conductance similar to an ion channel. *J Cell Biol* 129:99–104.
37. Albillos A, et al. (1997) The exocytotic event in chromaffin cells revealed by patch amperometry. *Nature* 389:509–512.

NEUROSCIENCE